The Astrophysical Journal Letters, 943:L18 (8pp), 2023 February 1 https://doi.org/10.3847/2041-8213/acaf67

Linear and Circular Polarimetry of the Optically Bright Relativistic Tidal Disruption Event AT 2022cmc

Aleksandar Cikota[1,2], Giorgos Leloudas[3], Mattia Bulla[4,5,6], Lixin Dai[7], Justyn Maund[8], and Igor Andreoni[9,10,11,12]
[1] Gemini Observatory/NSF's NOIRLab, Casilla 603, La Serena, Chile; aleksandar.cikota@noirlab.edu
[2] European Organisation for Astronomical Research in the Southern Hemisphere (ESO), Alonso de Cordova 3107, Vitacura, Casilla 19001, Santiago de Chile, Chile
[3] DTU Space, National Space Institute, Technical University of Denmark, Elektrovej 327, DK-2800 Kgs. Lyngby, Denmark
[4] Department of Physics and Earth Science, University of Ferrara, via Saragat 1, I-44122 Ferrara, Italy
[5] INFN, Sezione di Ferrara, via Saragat 1, I-44122 Ferrara, Italy
[6] INAF, Osservatorio Astronomico d'Abruzzo, via Mentore Maggini snc, I-64100 Teramo, Italy
[7] Department of Physics, The University of Hong Kong, Pokfulam Road, Hong Kong
[8] Department of Physics and Astronomy, The University of Sheffield, Hicks Building, Hounsfield Road, Sheffield, S3 7RH, UK
[9] Joint Space-Science Institute, University of Maryland, College Park, MD 20742, USA
[10] Department of Astronomy, University of Maryland, College Park, MD 20742, USA
[11] Astrophysics Science Division, NASA Goddard Space Flight Center, Mail Code 661, Greenbelt, MD 20771, USA
Received 2022 November 6; revised 2022 December 30; accepted 2023 January 1; published 2023 January 31

Abstract

Tidal disruption events (TDEs) occur when a star orbiting a massive black hole is sufficiently close to being tidally ripped apart by the black hole. AT 2022cmc is the first relativistic TDE that was observed (and discovered) as an optically bright and fast transient, showing signatures of nonthermal radiation induced by a jet that is oriented toward the Earth. In this work, we present optical linear and circular polarization measurements, observed with the Very Large Telescope/FORS2 in the *R* band (which corresponds to the blue/UV part of the spectrum in the rest frame), ∼7.2 and ∼12.2 rest-frame days after the first detection, respectively, when the light curve of the transient had settled in a bright blue plateau. Both linear and circular polarizations are consistent with zero, $p_{\rm lin} = 0.14\% \pm 0.73\%$, and $p_{\rm cir} = -0.30\% \pm 0.53\%$. This is the highest signal-to-noise ratio linear polarization measurement obtained for a relativistic TDE and the first circular polarimetry for such a transient. The nondetection of the linear and circular polarizations is consistent with the scenario of AT 2022cmc being a TDE where the thermal component (disk+outflows) is viewed pole-on, assuming an axially symmetric geometry. The presence and effect of a jet and/or external shocks are, however, difficult to disentangle.

Unified Astronomy Thesaurus concepts: Tidal disruption (1696); Polarimetry (1278); High energy astrophysics (739); Relativistic jets (1390)

1. Introduction

Tidal disruptions of stars around supermassive black holes (Rees 1988; Phinney 1989) have been discovered using a variety of methods at different wavelengths (Komossa & Bade 1999; Gezari et al. 2006; Levan et al. 2011; Gezari et al. 2012). Nowadays, the majority of tidal disruption events (TDEs) are found by wide-field optical surveys, and a distinct class of objects has been discovered where the optical/UV emission is dominated by a thermal component with blackbody temperatures 2–4 $\times 10^4$ K (van Velzen et al. 2020). While these objects, primarily found in quiescent or poststarburst galaxies (Arcavi et al. 2014; French et al. 2020), constitute the most numerous and homogeneous class among TDEs, there exist a number of other transients that have been proposed to be due to tidal disruptions. These include objects found through their X-ray emission (Saxton et al. 2020); objects found in active galactic nuclei (AGNs; explicitly excluded by the criteria of van Velzen et al. 2020), such as PS16dtm (Blanchard et al. 2017); objects found in luminous infrared galaxies often suffering considerable extinction (Tadhunter et al. 2017; Mattila et al. 2018); unique objects such as the superluminous ASASSN-15lh (Leloudas et al. 2016), some of which are often debated to be of supernova or AGN origin (see Zabludoff et al. 2021); or fast blue optical transients (FBOTs), such as AT 2018cow, whose nature is also debated (e.g., Kuin et al. 2019; Perley et al. 2019; Kremer et al. 2021; Liu et al. 2022; Metzger 2022).

Within the TDE zoo, there also exist a small number of objects that have been discovered through their high-energy emission by triggering the Burst Alert Telescope on the Neil Gehrels Swift Observatory. These include Swift J164449.3 +57345 (Bloom et al. 2011; Levan et al. 2011; Zauderer et al. 2011), Swift J2058.4+0516 (Cenko et al. 2012; Pasham et al. 2015), and Swift J1112.2-8238 (Brown et al. 2015). These transients, found typically at higher redshifts (up to $z \sim 1.2$), exhibit strong and long-lasting X-ray emission with rapid variability (differentiating them from gamma-ray burst, GRB, afterglows), accompanied by radio emission attributed to synchrotron radiation. The consensus is that these objects are TDEs that are thought to have relativistic jets and for this reason, are also known as relativistic or "jetted" TDEs.

AT 2022cmc is another transient at $z = 1.193$ (Tanvir et al. 2022) that has been proposed to be a relativistic TDE (Andreoni et al. 2022a; Pasham et al. 2023) although it was not discovered through its high-energy emission. It was discovered in the optical by a wide-field transient survey, the Zwicky Transient Facility (Bellm et al. 2019), where it was

[12] Neil Gehrels Fellow.

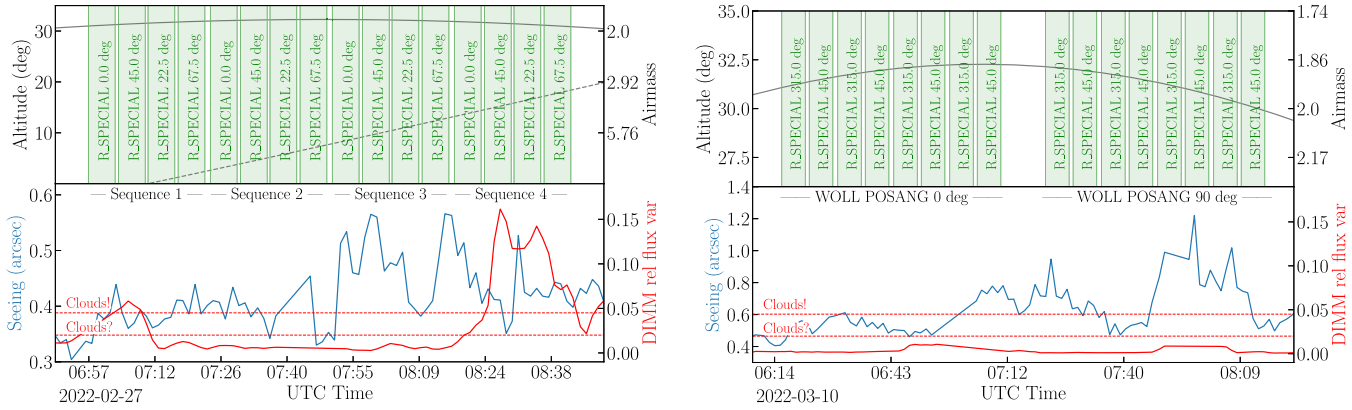

Figure 1. Observing log of linear and circular polarimetry of AT 2022cmc. The green blocks on the top panels indicate the individual exposures, each of 350 s in the *R* band, and the corresponding HWP angles. The solid and dashed lines show the altitudes of the target and Moon, respectively. The bottom panels show the seeing measured by the Astronomical Site Monitoring (ASM) DIMM telescope at 500 nm (blue line) and the relative flux variation along the line of sight of the DIMM telescope (solid red line) during the observations. The dashed red lines indicate thresholds for the possible presence of clouds. Left: the linear polarimetry sequence of four HWP angles was repeated four times to increase the S/N. The individual sequences are indicated. Right: circular polarimetry was obtained at two orientations of the instrument, separated by 90°. At each orientation, four sequences of two quarter-wave plate positions were taken.

initially noticed as a fast and red transient (Andreoni et al. 2022b). Andreoni et al. (2022a) presented a detailed study of this event for the first 15 rest-frame days, including X-ray, UV/optical/IR, and submillimeter/radio data, suggesting that a relativistic jet was formed, producing an afterglow powered by synchrotron radiation. In the UV/optical wavelengths, they showed that the initial rapid (and red) decay phase is followed by a bluer luminous ($M_g \sim -22$ mag) plateau ∼4.5 days after detection in the rest frame (∼10 days in observer frame; see their Figure 1), and they argue that this second phase traces a more ordinary thermal component, reminiscent of optical TDEs. Andreoni et al. (2022a) examined alternative solutions for the nature of this transient, including a kilonova, FBOT, and a GRB origin, but they reject all of them supporting the scenario of a relativistic TDE. This conclusion is corroborated by Pasham et al. (2023) who show that the X-ray emission of AT 2022cmc demonstrates rapid variability on timescales of hours, requiring a small emitting region, seen previously in relativistic TDEs but not in GRB afterglows. Their spectral energy distribution (SED) modeling shows that the X-rays are more likely produced through synchrotron self-Compton (SSC) emission, while radio emission is standard synchrotron emission. A clear thermal component dominates in the optical/UV at ∼11 days in the rest frame (∼25 days in the observer frame; see their Figure 3).

Here we present optical (rest-frame UV) linear and circular polarimetry of AT 2022cmc obtained at 15.84 and 26.81 observer-frame days (7.22 and 12.23 rest-frame days), respectively, relative to the first detection on 2022 February 11 at 10:42:40 UTC (MJD 59621.44), following Andreoni et al. (2022a). Thus, the blue plateau dominates the transient evolution during our observed epochs.

In Section 2 we explain the observations, in Section 3 we present the methods and results, and in Section 4 we discuss our results in the context of the proposed scenarios for this transient. Section 5 contains our summary and concluding remarks.

2. Observations

We obtained imaging linear and circular polarimetry of AT 2022cmc ($\alpha = 1\,3{:}34{:}43.207$, $\delta = +33{:}13{:}00.54$) on 2022 February 27 at 06:57 UT (MJD 59637.29) and 2022 March 10 at 06:16 UT (MJD 59648.26), respectively, with the FORS2 (Appenzeller et al. 1998) mounted on the primary focus of European Southern Observatory's (ESO) Very Large Telescope (VLT), Antu (UT1). All observations were obtained using the FORS2 R_SPECIAL filter ($\lambda_0 = 655$ nm, FWHM = 165 nm), which corresponds to the central wavelength of $\lambda_0 = 299$ nm at $z = 1.193$. The brightness of AT 2022cmc at these phases was 21.8 ± 0.4 *R* mag and 22.0 ± 0.4 *R* mag, measured with aperture photometry in the FORS2 acquisition images using the Vega photometric system.

Figure 1 shows the observing log with individual exposures for the linear polarization (left panel) and circular polarization observations (right panel). The seeing conditions, measured with the differential image motion monitor (Sarazin & Roddier 1990; DIMM), have been downloaded from the Ambient Conditions Database.[13]

Linear polarimetry was acquired using four half-wave plate (HWP) angles of 0°, 22.°5, 45°, and 67.°5, and repeated four times to increase the signal-to-noise ratio (S/N). The redundancy of four HWP angles reduces the flat-fielding issue and cancels out other instrumental effects (see Patat & Romaniello 2006). AT 2022cmc was at its peak altitude during the observations, between ∼30 and ∼33°, at an air mass of just above 2. The seeing was stable during the observations, between ∼0.″3 and 0.″6, and the sky transparency determined by the weather officer was clear; however, during the fourth sequence, there were some thin clouds passing (see Figure 1). The measured FWHM of the target was between ∼0.″7 and 0.″9 during the observations. The Moon, at a distance of ∼105° from AT 2022cmc and on illumination of 15%, started rising at ∼07:00 UT and reached an altitude of ∼20° by the end of the observations.

Circular polarimetry was obtained with two different quarter-wave retarder plate (QWP) angles of ±45°. The sequence of two QWP angles has been repeated four times to increase the S/N. Furthermore, the set of 4 × 2 angles has been taken at two different rotations of the instrument of 0° and 90° in order to eliminate possible cross talk between linear and circular polarizations (see Bagnulo et al. 2009). The target was again observed during its peak altitude, at an air mass of $\lesssim 2$ and with

[13] http://archive.eso.org/cms/eso-data/ambient-conditions.html

the Moon set. The sky transparency was clear during the execution of the observing block; however, the seeing was variable and increased up to ∼1.″2 during the second set of observations with the instrument rotated. The measured FWHM of the target was between ∼0.″9 and 1.″2 during the observations.

3. Methods and Results

3.1. Linear Polarimetry

To calculate the linear polarization of AT 2022cmc, we measured the flux of the target in the ordinary and extraordinary beams at all HWP angles using the aperture photometry function from PythonPhot.[14] We used an aperture radius of 1.″3, with the inner and outer sky radii of 2.″5 and 5″, respectively. Tests with slight variations of the aperture and sky radii produced consistent results. The aperture sizes and positions were fixed for all images within the sequences.

The normalized Stokes q and u parameters were calculated following the standard approach as described in the FORS2 User Manual (Anderson 2015; see also Cikota et al. 2017; Chu et al. 2022):

$$q = \frac{2}{N}\sum_{i=0}^{N-1} F(\theta_i)\cos(4\theta_i),$$
$$u = \frac{2}{N}\sum_{i=0}^{N-1} F(\theta_i)\sin(4\theta_i), \quad (1)$$

where N ranges over the half-wave retarder plate angle, $\theta_i = 22.^{\circ}5 \times i$, with $0 \leqslant i \leqslant 3$, and $F(\theta_i)$ is the normalized flux difference between the ordinary (f^o) and extraordinary (f^e) beams:

$$F(\theta_i) = \frac{f^o(\theta_i) - f^e(\theta_i)}{f^o(\theta_i) + f^e(\theta_i)}. \quad (2)$$

The polarization position angles of the raw measurements have been corrected for the HWP zero angle chromatic dependence (Table 4.7 in Anderson 2015).

The reduction pipeline and possible instrumental effects (i.e., instrumental polarization and angle offset) have been verified using archival observations of polarized and unpolarized standard stars.

The measured Stokes parameters for AT 2022cmc are $q = 0.20\% \pm 0.67\%$ and $u = 0.17\% \pm 0.79\%$, which lead to a polarization degree of $p_{\rm lin} = 0.26\% \pm 0.73\%$, and after a polarization bias correction, following Plaszczynski et al. (2014), $p_{\rm lin_{BiasCorr}} = 0.14\% \pm 0.73\%$, i.e., a 3σ upper limit of ∼2.3%. We note that the host galaxy of AT 2022cmc is not detected to very faint limits (>24.5 mag; Andreoni et al. 2022a), and it can therefore contribute a maximum 6% of the captured light. For this reason, we have not applied any host galaxy dilution correction for the transient polarization (Leloudas et al. 2022; Liodakis et al. 2022b).

The polarization of AT 2022cmc is shown on the Stokes q–u plane in Figure 2. The main plot shows the polarization determined from all data combined, i.e., by calculating the normalized flux difference for each HWP angle using all four sequences of the four HWP angles before calculating the Stokes q and u.

The small subplots at the top of Figure 2 display the polarization of AT 2022cmc measured using the individual sequences (which consists of four HWP angles). All the measurements are consistent with zero polarization. The measurement in Sequence 4 has been affected by thin clouds passing (see Figure 1) and therefore exhibits larger error bars and a larger offset compared to the first three sequences. If we exclude the last sequence and determine the polarization from the first three sequences only, the result remains consistent within the uncertainties.

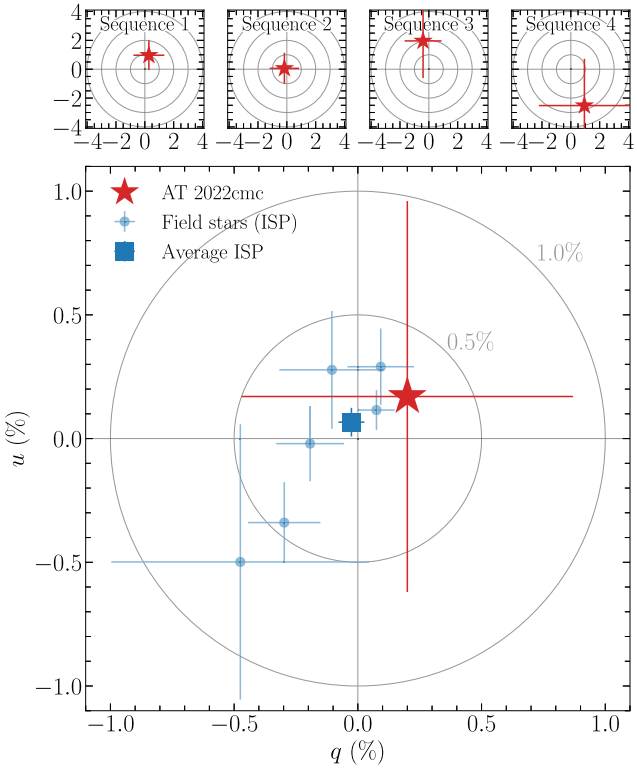

Figure 2. Linear polarization of AT 2022cmc (red star) in the Stokes q–u plane at 7.22 rest-frame days after first detection. The light blue circles display the ISP measured through field stars, and the blue square is their weighted mean. The polarization of AT 2022cmc measured in the individual sequences is displayed in the four subplots on the top of the figure. The gray concentric circles in the subplots denote polarization degrees of 1%, 2%, 3%, and 4%. The polarization of AT 2022cmc is consistent with zero, and this is also true for the ISP.

In addition, we used six bright field stars to determine the interstellar polarization (ISP) by calculating their weighted mean in the q–u plane (Figure 2). We corrected the field stars' polarization measurements for the instrumental polarization (Patat & Romaniello 2006; González-Gaitán et al. 2020), which increases with distance from the optical axis, using the same methods as applied in Chu et al. (2022, see their Figure 2) and Leloudas et al. (2015). The mean ISP determined from the field stars is negligible, $p_{\rm lin} = 0.03\% \pm 0.06\%$. This is consistent with the low values found for nearby stars in the catalog by Heiles (2000) and with the low Galactic reddening, $E(B-V) = 0.0095 \pm 0.0006$ mag, in the direction of AT 2022cmc (Schlafly & Finkbeiner 2011).

Andreoni et al. (2022a) suggest that AT 2022cmc does not suffer from any significant host extinction. Therefore, we also do not expect significant host galaxy ISP, which is also consistent with the nondetection of linear polarization.

[14] https://github.com/djones1040/PythonPhot

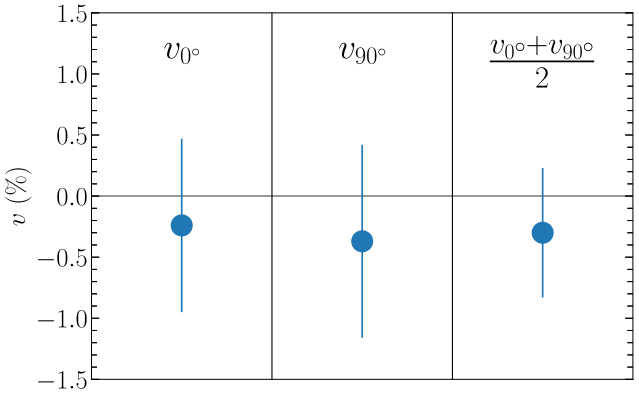

Figure 3. Circular polarization of AT 2022cmc at 12.23 days after first detection in the rest frame. The left and middle panels show the circular polarization measured at two different orientations of the instrument, separated by 90°, and the right panel shows the average of both measurements. The circular polarization is consistent with zero.

3.2. Circular Polarimetry

The flux of AT 2022cmc was extracted from the ordinary and extraordinary beams using the same tools as described in the previous section (Section 3.1), and the amount of circular polarization was calculated following the equation for the Stokes v given in the FORS2 User Manual (Anderson 2015):

$$v = \frac{1}{2}\left[\left(\frac{f^o - f^e}{f^o + f^e}\right)_{\theta=45°} - \left(\frac{f^o - f^e}{f^o + f^e}\right)_{\theta=-45°}\right], \quad (3)$$

where f^o and f^e are the fluxes measured in the ordinary and extraordinary beams, respectively, for both QWP angles of $\theta = \pm 45°$. For circular polarimetry, we used an aperture radius of $1\farcs5$, with the inner and outer sky radii of $2\farcs5$ and $5''$, respectively.

Figure 3 displays the circular polarization measured at two different orientations of the instrument separated by 90° (left and middle panels). The two measurements of $v_{0°} = -0.24\% \pm 0.71\%$ (observed with the instrument aligned toward the north celestial pole) and $v_{90°} = -0.37\% \pm 0.79\%$ (observed with the instrument rotated by 90°) are consistent. Furthermore, the weighted average of the two measurements, which benefits from the cancellation of the possible spurious signal (introduced because of linear-to-circular polarization cross talk; see Bagnulo et al. 2009) is $p_{\rm cir} = -0.30\% \pm 0.53\%$ (right panel in Figure 3). Thus, we did not detect significant circular polarization for AT 2022cmc. Note that in the case of circular polarimetry no bias correction is needed, in contrast to linear polarimetry.

4. Discussion

Optical polarimetry has been extensively used in order to probe the geometry and physics of transients. The origin and degree of polarization vary for different transients and physical mechanisms. In supernova explosions, the polarization is primarily produced due to electron scattering (i.e., Thomson scattering), and the degree of the continuum polarization is related to the degree of asymmetry of the photosphere (Hoflich 1991; Kasen et al. 2003). Continuum polarization levels range from <0.3% for Type Ia supernovae (SNe Ia), indicating they are nearly spherical (Cikota et al. 2019), and up to 1%–2% for core-collapse supernovae (SNe), with stripped Type Ib/c supernovae (SNe Ib/c) being the most asymmetric (Wang & Wheeler 2008; Patat 2017). Very few circular polarimetry measurements have been obtained, and observations of two superluminous supernovae (SLSNe) and an SN Ia only resulted in nondetections (Maund et al. 2013; Cikota et al. 2018). Despite the very different opacities and their critical role, electron scattering is also expected to be the source of polarization in kilonovae from neutron star mergers (Bulla et al. 2019, 2021), and AT 2017gfo, related to GW170817, showed very low polarization levels likely due to ISP (0.5%; Covino et al. 2017).

For GRBs, on the other hand, there are several mechanisms that could cause polarization (Covino & Gotz 2016). Although in the first few minutes, linear polarization values of up to 30% induced by reverse shocks have been reported (Mundell et al. 2013), values between 0% and 3% have been observed on timescales of hours and days after several GRBs, showing moderate variability with a generally decreasing trend. The afterglow polarization is attributed to synchrotron emission from shock-accelerated electrons in the ambient medium (forward shock). The measured polarization is strongly dependent on the geometric configuration, whether the viewing angle is within the jet opening angle, the structure of the jet, or the nature (ordered versus random) of the magnetic fields (see, e.g., Rossi et al. 2004; Lazzati 2006; Stringer & Lazzati 2020; Teboul & Shaviv 2021). The polarization is expected to peak at the jet-break time. Circular polarimetry of GRBs has mostly yielded upper limits, with the exception of a $0.61\% \pm 0.13\%$ detection for GRB 121024A (Wiersema et al. 2014). Also in the case of blazars 3C 279 and PKS 1510-089, which show variable and high levels of linear polarization in the optical wavelengths (between 0 and >30%), no obvious circular polarization was detected ($p_{\rm cir} < 1\%$, Liodakis et al. 2022a).

Polarimetry of TDEs is a nascent field. Interestingly, some of the first studies were made for the rare class of relativistic TDEs. Wiersema et al. (2012) measured $7.4\% \pm 3.5\%$ in the K_s band for Swift J164449.3+57345 at 12.2 rest-frame days after trigger (note that the time of trigger approximately coincides to peak brightness for fast transients). This event was, however, highly extincted in the optical, and it is not clear how much polarization induced by dust affects this result. Nevertheless, the authors seem to disfavor the contribution from an SSC component in the K-band polarization, even if the presence of such a component is suggested by SED modeling (Bloom et al. 2011). Furthermore, Wiersema et al. (2020) presented optical linear polarimetry of Swift J2058.4+0516, which did not suffer from significant extinction. They report $p_{\rm lin} < 5.3\%$ and $p_{\rm lin} = 8.1\% \pm 2.5\%$ at 40 and 75 days after trigger in the rest frame, respectively. We note that these were challenging measurements, even for the VLT, as the transient was 23–24 mag at the time of observations, which is reflected in the low S/N. This polarization could originate from synchrotron radiation from the forward shock in the jet although these values are larger than what are seen for GRBs at these phases. Another exceptionally luminous transient (likely a TDE as argued in Leloudas et al. 2016 although a superluminous supernova origin has also been proposed by Dong et al. 2016) with a good polarimetric coverage is ASASSN-15lh (Maund et al. 2020). This object shows an overall constant polarization level of ∼0.4% between +30 and +90 days relative to peak brightness in the rest frame with a single individual measurement showing

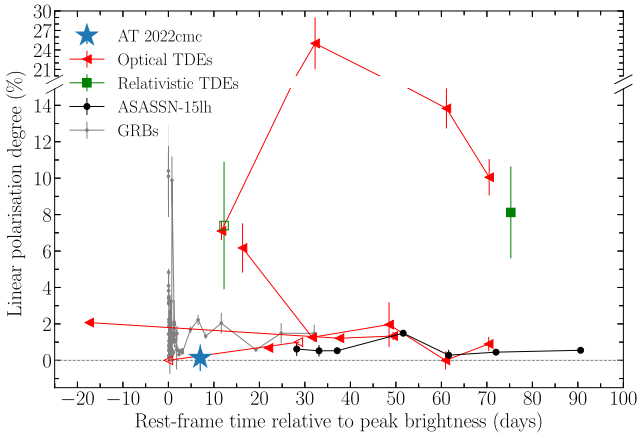

Figure 4. Linear polarization of AT 2022cmc (this work, blue star) compared to the polarization of TDEs AT 2018dyb, AT 2019dsg, AT 2019azh, AT 2019qiz, and AT 2020mot (Leloudas et al. 2022; Patra et al. 2022; Liodakis et al. 2022b; red triangles); relativistic TDEs Swift J164449.3+573451 and Swift J2058+0516 (Wiersema et al. 2012, 2020; green squares); the superluminous transient ASASSN-15lh (Maund et al. 2020; black circles); and GRBs collected by Covino & Gotz (2016; gray circles) with $N > 4$ epochs. The polarization is shown as a function of days relative to peak brightness. Note that the time of first detection approximately coincides to peak brightness for GRBs. TDEs J164449.3+57345 and AT 2019qiz are marked with open symbols to mark uncertain values because they have not been corrected for the host galaxy dilution (see Section 4).

$p_{\rm lin} = 1.2\% \pm 0.2\%$ near the minimum of the UV light curve, indicating possible rapid variability in timescales of ± 10 days. Spectral polarimetry indicates a polarization level that is overall independent of wavelength.

Polarimetric observations of "ordinary" optical TDEs (van Velzen et al. 2020) were scarce until recently, including few measurements of individual events (Higgins et al. 2019; Lee et al. 2020; Holoien et al. 2020). Leloudas et al. (2022) gathered spectral polarimetry for a sample of three optical TDEs and demonstrated that the continuum polarization is wavelength independent, while emission lines depolarize the spectrum. They suggest that the origin of polarization in optical TDEs is electron scattering, similar to SNe and kilonovae, and they exclude synchrotron radiation and dust scattering as significant contributors. The polarization is observed to decrease with time, and Leloudas et al. (2022) propose that the data is compatible with the formation and evolution of a super-Eddington accretion disk. They further model the polarization with the super-Eddington accretion model of Dai et al. (2018) and the radiative transfer code POSSIS (Bulla 2019), yielding polarization predictions between 0% and 6% for different observing angles, values that are broadly consistent with the observations. A simultaneous study (Patra et al. 2022) presented spectral polarimetry of AT 2019qiz, showing zero polarization at peak but increasing with time, one month later. Finally, the study by Liodakis et al. (2022a) presented time-varying polarization for AT 2020mot, reaching an extraordinary $25\% \pm 4\%$ in one epoch. This measurement is very hard to explain by reprocessing models (Charalampopoulos et al. 2022; Leloudas et al. 2022), and the authors favor shock collisions for this TDE.

Figure 4 shows a comparison of the linear polarization of AT 2022cmc with other transients, including ordinary optical TDEs (Leloudas et al. 2022; Liodakis et al. 2022b; Patra et al. 2022), relativistic (Wiersema et al. 2012, 2020) and extreme TDEs (ASASSN-15lh; Maund et al. 2020), and a sample of GRBs selected from Covino & Gotz (2016) with N > 4 epochs.

We note that the nuclear transients in this figure have either been corrected for host dilution (Leloudas et al. 2022; Liodakis et al. 2022b)[15] or such a correction is not necessary, as in the case of Swift J2058+0516 and AT 2022cmc, where the transient was >3 mag brighter than the host at the time of linear polarimetry (Pasham et al. 2015; Andreoni et al. 2022a). Two transients have not been host corrected due to limited or unavailable information and appear in Figure 4 with open symbols. These are AT 2019qiz (Patra et al. 2022) and Swift J164449.3+57345 (Wiersema et al. 2012). In the first case, the 0% value at peak will not be affected, but the 1% one month later is a lower limit. The case of Swift J164449.3+57345 is much more complicated as the intrinsic polarization is both uncertain due to the host contribution but also due to considerable contribution by dust (Wiersema et al. 2012). The GRB literature data is not host corrected, but we expect this correction to not be significant as GRBs are not embedded in their host galaxy nucleus, and their afterglows typically outshine the host.

4.1. The Unpolarized Case of AT 2022cmc

The optical/near-infrared (NIR) light curve of AT 2022cmc displays a steep decrease in brightness from ∼19.0 mag to ∼21.5 mag in the r band the first ∼5 days (in the rest frame) and a plateau after the ∼5th day, which lasts at least until the 15th day, followed by a slower decrease (Andreoni et al. 2022a). Both linear and circular polarimetry of AT 2022cmc was obtained during that plateau phase, where the optical light is dominated by a blue component.

The degree of linear polarization is very low at $p_{\rm lin} = 0.14\% \pm 0.73\%$, consistent with zero, and lower than what has been observed in the case of the other two relativistic TDEs, Swift J164449.3+573451 and Swift J2058+0516. It is also lower than the linear polarization measured for 3/5 optical TDEs at 97% confidence. The spectrum of AT 2022cmc is featureless (Figure 3 in Andreoni et al. 2022a) during the phases of our observations, so a contribution due to depolarizing emission lines (Leloudas et al. 2022; Patra et al. 2022) can be excluded.

In general, optical linear polarization in TDEs can be produced by at least the following mechanisms: (i) By the synchrotron radiation of an on-axis or off-axis jet, as in the case of GRBs or blazars. This has been proposed for previous relativistic TDEs (Wiersema et al. 2012, 2020). Note that in the case of jets we also expect detection of radio and/or X-rays, which was observed in the case of AT 2022cmc (Andreoni et al. 2022a; Pasham et al. 2023); (ii) Stellar stream shocks can produce high polarization degrees (>25%), which arise as the result of multiple competing shocks. This was proposed in the case of AT 2020mot (Liodakis et al. 2022a); and (iii) Electron scattering from a reprocessing layer in an accretion disk and possible outflows. In the case of the super-Eddington accretion disk model of Dai et al. (2018), the polarization is expected to decrease with the viewing angle and can reach polarization degrees of up to ∼6% for edge-on disks, depending also on the

[15] The data for ASASSN-15lh was not host corrected in Maund et al. (2020), but we applied the correction here for the first time. We find that the host contamination in the V band is small and increases from 13% to 24% during the polarimetric observations. This minor correction does not affect the discussion in Maund et al. (2020).

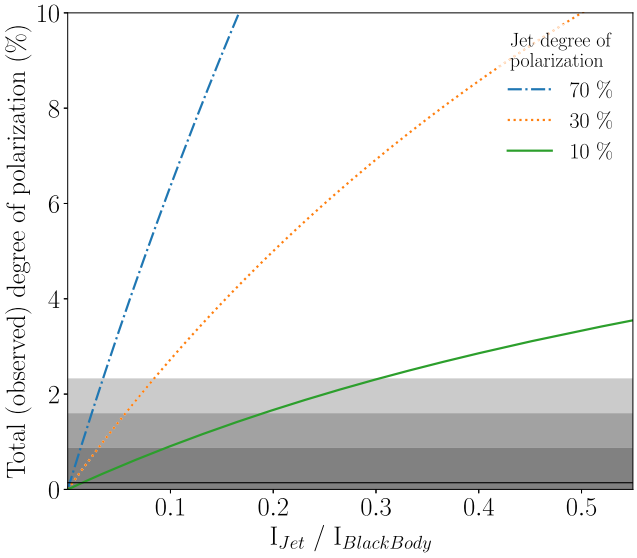

Figure 5. Constraints to the ratio of the nonthermal to the thermal component for AT 2022cmc at 7.2 days, based on our linear polarimetry observations and the degree of polarization of the putative jet. The black line shows the measured linear polarization of 0.14%, and the gray shaded areas indicate the 1σ, 2σ, and 3σ uncertainties.

density distribution of the material in the disk (Leloudas et al. 2022). Note that there is a variety of possible TDE accretion models, which may produce different polarization degrees, including the collision-induced outflow (Lu & Bonnerot 2020), which can produce linear polarization up to 9% (Charalampopoulos et al. 2022), or the zero-Bernoulli accretion flow model (Coughlin & Begelman 2014), which assumes that an accretion disk is quasispherical, radiation-pressure dominated, and accompanied by the production of strong jets (Eyles-Ferris et al. 2022). Furthermore, clumpy flared disk models may produce higher polarization degrees of up to ∼10% and variable polarization angles (Marin & Stalevski 2015). Such reprocessed radiation is also expected to be detectable in the radio wavelengths.

It is therefore difficult to confidently exclude any models based on a single measurement of $p_{\rm lin} < 2.3\%$, especially when this is compatible with zero polarization, which could be realized for specific viewing angles. What is, however, possible is to confirm that the zero polarization is consistent with the POSSIS modeling in Leloudas et al. (2022) for a TDE accretion flow viewed relatively close to the pole. This idea is therefore compatible with the scenario proposed by Andreoni et al. (2022a), where at these phases the optical/UV probes a thermal component (outflows) from the TDE. This, however, assumes an axisymmetric geometry, as in the (idealized) model.

In addition, this ignores any contribution from the jet in the UV/optical already at 7.2 days after discovery. This may either mean that the jet component is subdominant or that the jet is not significantly intrinsically polarized. This is illustrated in Figure 5, which shows the predicted polarization levels, assuming different ratios of the two components and different levels of polarization for the putative jet component, ranging from 10% to the maximum theoretical value of 70% for synchrotron radiation (Granot 2003; Granot & Knigl 2003; Nakar et al. 2003; see also Covino & Gotz 2016 for a review). However, that is not the case for GRB afterglows, in which the emission is produced by shocked ambient medium (forward shock), and the intrinsic polarization averages out in the magnetic fields, which appears random to the observer. Thus, despite the fact that polarization in GRB afterglows is produced due to synchrotron emission, the measured polarization is strongly dependent on the geometric nature, with only a small contribution from ordered fields. Due to relativistic effects in the observed geometry of the blastwave (i.e., the surface of equal arrival time; see Granot & Ramirez-Ruiz 2010), the detection of small levels of polarization in afterglows seen on-axis (i.e., the viewing angle is within the jet opening angle) is not surprising (see Figure 3 in Lazzati 2006; see also Matsumiya & Ioka 2003; Sagiv et al. 2004; Toma et al. 2008; Hutsemékers et al. 2010; Liodakis et al. 2022a). In the case of afterglows seen off-axis, the magnetic fields normal to the blastwave become more important (e.g., Gill & Granot 2020). Because the observed polarization mostly depends on the geometry, as the blastwave decelerates, the polarization is predicted to change with time, in a way that depends on the viewing angle, the jet opening angle (which also captures the Lorentz factor), the emission structure of the jet, and the presence of ordered fields (see, e.g., Rossi et al. 2004; Stringer & Lazzati 2020; Teboul & Shaviv 2021). The closer we are observing relative to the jet axis and/or the longer away from the jet-break time (around which the polarization is expected to peak) we are observing, the lower the linear polarization is expected to be. It is therefore obvious that several intrinsic polarization values in Figure 5 are unrealistic. This figure is, however, model free and has the aim to visualize the different possible contributions of a jet component at 7.2 days for different intrinsic polarizations. This may be useful because the exact contribution of the nonthermal component (which was dominant in the first days) is difficult to constrain in the optical regime, based on the light-curve decomposition or SED modeling alone (Andreoni et al. 2022a; Pasham et al. 2023). For instance, Figure 5 shows that a jet polarized at the 10% level (not very different from the measurements obtained for the previous relativistic TDEs) cannot contribute more than 30% than the thermal component at 7.2 days.

Pasham et al. (2023) also suggested that the high-energy emission (X-ray) originates from inverse-Compton scattering (either SSC or external Compton). Inverse-Compton is expected to produce nonintrinsic circular polarization in the case of a jet that is not made of pure electron–positron plasma but also contains some fraction of protons (Liodakis et al. 2022a). The degree of circular polarization depends on the strength of the magnetic field, the observing frequency, the uniformity of the magnetic field (which can be measured through the degree of linear polarization), the fraction of positrons, and the Lorentz factor (see Equation (1) in Liodakis et al. 2022a). However, from the nondetection of significant circular and linear polarizations in the case of AT 2022cmc, the ratio $p_{\rm cir}/p_{\rm lin}$ diverges, and we cannot make any conclusions on the strength of the magnetic field and the fraction of positrons. We note that radio polarimetry would be more relevant for studies of jet properties in TDEs, compared to optical polarimetry. Matsumiya & Ioka (2003) calculated that, in the presence of an ordered magnetic field, the intrinsic circular polarization of synchrotron emission can reach 1% for forward shocks and 10%–1% for reverse shocks at radio frequencies, in contrast to 0.01% and 0.1%–0.01% at optical frequencies, respectively (see also Wiersema et al. 2012). At face value, however, the polarization measurements seem compatible with

the modeling of Pasham et al. (2023), who favor a matter-dominated jet with low magnetic field energy density. The nondetection of circular polarization may also imply no anisotropic pitch-angle distribution, which may produce circular polarization also in the case of random magnetic field orientations (see, e.g., Wiersema et al. 2014). Furthermore, in forward shocks, ordered magnetic fields originating from the central engine are not likely (Matsumiya & Ioka 2003; Sagiv et al. 2004; Mundell et al. 2013; Wiersema et al. 2014), which is also consistent with the nondetection of circular polarization.

Therefore, the low observed linear and circular polarization degrees are compatible with the suggested explanations by Andreoni et al. (2022a) and Pasham et al. (2023) that AT 2022cmc is a relativistic TDE seen pole-on, that the optical/UV is dominated by a thermal component during the plateau phase, and that the jet is possibly matter dominated.

5. Summary and Conclusions

Linear and circular polarimetry of AT 2022cmc was performed with VLT/FORS2 in the *R* band during the plateau phase, on 2022 February 27 and 2022 March 10 (7.22 and 12.23 rest-frame days after the detection), respectively. Neither obvious linear nor circular polarization was detected. The linear polarization degree is $p_{\rm lin} = 0.14\% \pm 0.73\%$, with a 3σ upper limit of 2.3%, and the circular polarization degree is $p_{\rm cir} = -0.30\% \pm 0.53\%$.

The nondetection of polarization is consistent with the scenario that AT 2022cmc is a relativistic TDE and that, at the phases obtained, the observed emission most likely originates from a thermal component from the TDE that is axially symmetric and is viewed pole-on.

Next-generation time-domain surveys (e.g., the Vera C. Rubin Observatory) will allow us to detect a large sample of TDEs and other transients in the near future. Our work demonstrates that it is important to conduct spectropolarimetric observations of the fast-fading optical components of new (jetted) TDEs in real time, as this can help us probe the structure of the gas flow and constrain the origin of TDE emissions (Roth et al. 2020; Dai et al. 2021).

This work is based on observations collected at the European Organisation for Astronomical Research in the Southern Hemisphere under ESO program 108.222Q.001 (PI Leloudas); the execution in service mode of these observations by the VLT operations staff is gratefully acknowledged. The work of A.C. is supported by NOIRLab, which is managed by the Association of Universities for Research in Astronomy (AURA) under a cooperative agreement with the National Science Foundation. G.L. was supported by a research grant (19054) from VILLUM FONDEN. M.B. acknowledges support from the European Union's Horizon 2020 Programme under the AHEAD2020 project (grant agreement n. 871158). L.D. acknowledges the support from the Hong Kong Research Grants Council (HKU27305119, HKU17304821) and the National Natural Science Foundation of China (HKU12122309). We thank the anonymous referee for constructive comments.

ORCID iDs

Aleksandar Cikota https://orcid.org/0000-0001-7101-9831
Giorgos Leloudas https://orcid.org/0000-0002-8597-0756
Mattia Bulla https://orcid.org/0000-0002-8255-5127
Lixin Dai https://orcid.org/0000-0002-9589-5235
Justyn Maund https://orcid.org/0000-0003-0733-7215
Igor Andreoni https://orcid.org/0000-0002-8977-1498

References

Anderson, J. 2015, FORS2 User Manual (Garching: ESO), http://www.eso.org/sci/facilities/paranal/instruments/fors/doc/VLT-MAN-ESO-13100-1543_P01.1.pdf
Andreoni, I., Coughlin, M., Ahumada, T., et al. 2022b, TNSAN, 38, 1
Andreoni, I., Coughlin, M. W., Perley, D. A., et al. 2022a, Natur, 612, 430
Appenzeller, I., Fricke, K., Fürtig, W., et al. 1998, Msngr, 94, 1
Arcavi, I., Gal-Yam, A., Sullivan, M., et al. 2014, ApJ, 793, 38
Bagnulo, S., Landolfi, M., Landstreet, J. D., et al. 2009, PASP, 121, 993
Bellm, E. C., Kulkarni, S. R., Graham, M. J., et al. 2019, PASP, 131, 018002
Blanchard, P. K., Nicholl, M., Berger, E., et al. 2017, ApJ, 843, 106
Bloom, J. S., Giannios, D., Metzger, B. D., et al. 2011, Sci, 333, 203
Brown, G. C., Levan, A. J., Stanway, E. R., et al. 2015, MNRAS, 452, 4297
Bulla, M. 2019, MNRAS, 489, 5037
Bulla, M., Covino, S., Kyutoku, K., et al. 2019, NatAs, 3, 99
Bulla, M., Kyutoku, K., Tanaka, M., et al. 2021, MNRAS, 501, 1891
Cenko, S. B., Krimm, H. A., Horesh, A., et al. 2012, ApJ, 753, 77
Charalampopoulos, P., Bulla, M., Bonnerot, C., & Leloudas, G. 2022, arXiv:2212.05079
Chu, M. R., Cikota, A., Baade, D., et al. 2022, MNRAS, 509, 6028
Cikota, A., Leloudas, G., Bulla, M., et al. 2018, MNRAS, 479, 4984
Cikota, A., Patat, F., Cikota, S., & Faran, T. 2017, MNRAS, 464, 4146
Cikota, A., Patat, F., Wang, L., et al. 2019, MNRAS, 490, 578
Coughlin, E. R., & Begelman, M. C. 2014, ApJ, 781, 82
Covino, S., & Gotz, D. 2016, A&AT, 29, 205
Covino, S., Wiersema, K., Fan, Y. Z., et al. 2017, NatAs, 1, 791
Dai, J. L., Lodato, G., & Cheng, R. 2021, SSRv, 217, 12
Dai, L., McKinney, J. C., Roth, N., Ramirez-Ruiz, E., & Miller, M. C. 2018, ApJL, 859, L20
Dong, S., Shappee, B. J., Prieto, J. L., et al. 2016, Sci, 351, 257
Eyles-Ferris, R. A. J., Starling, R. L. C., O'Brien, P. T., Nixon, C. J., & Coughlin, E. R. 2022, MNRAS, 517, 6013
French, K. D., Wevers, T., Law-Smith, J., Graur, O., & Zabludoff, A. I. 2020, SSRv, 216, 32
Gezari, S., Chornock, R., Rest, A., et al. 2012, Natur, 485, 217
Gezari, S., Martin, D. C., Milliard, B., et al. 2006, ApJL, 653, L25
Gill, R., & Granot, J. 2020, MNRAS, 491, 5815
González-Gaitán, S., Mourão, A. M., Patat, F., et al. 2020, A&A, 634, A70
Granot, J. 2003, ApJL, 596, L17
Granot, J., & Königl, A. 2003, ApJL, 594, L83
Granot, J., & Ramirez-Ruiz, E. 2010, arXiv:1012.5101
Heiles, C. 2000, AJ, 119, 923
Higgins, A. B., Wiersema, K., Covino, S., et al. 2019, MNRAS, 482, 5023
Hoflich, P. 1991, A&A, 246, 481
Holoien, T. W. S., Auchettl, K., Tucker, M. A., et al. 2020, ApJ, 898, 161
Hutsemékers, D., Borguet, B., Sluse, D., Cabanac, R., & Lamy, H. 2010, A&A, 520, L7
Kasen, D., Nugent, P., Wang, L., et al. 2003, ApJ, 593, 788
Komossa, S., & Bade, N. 1999, A&A, 343, 775
Kremer, K., Lu, W., Piro, A. L., et al. 2021, ApJ, 911, 104
Kuin, N. P. M., Wu, K., Oates, S., et al. 2019, MNRAS, 487, 2505
Lazzati, D. 2006, NJPh, 8, 131
Lee, C.-H., Hung, T., Matheson, T., et al. 2020, ApJL, 892, L1
Leloudas, G., Bulla, M., Cikota, A., et al. 2022, NatAs, 6, 1193
Leloudas, G., Fraser, M., Stone, N. C., et al. 2016, NatAs, 1, 0002
Leloudas, G., Patat, F., Maund, J. R., et al. 2015, ApJL, 815, L10
Levan, A. J., Tanvir, N. R., Cenko, S. B., et al. 2011, Sci, 333, 199
Liodakis, I., Blinov, D., Potter, S. B., & Rieger, F. M. 2022a, MNRAS, 509, L21
Liodakis, I., Koljonen, K. I. I., Blinov, D., et al. 2022b, arXiv:2208.14465
Liu, J.-F., Zhu, J.-P., Liu, L.-D., Yu, Y.-W., & Zhang, B. 2022, ApJL, 935, L34
Lu, W., & Bonnerot, C. 2020, MNRAS, 492, 686
Marin, F., & Stalevski, M. 2015, in SF2A-2015: Proceedings of the Annual meeting of the French Society of Astronomy and Astrophysics, 167
Matsumiya, M., & Ioka, K. 2003, ApJL, 595, L25
Mattila, S., Pérez-Torres, M., Efstathiou, A., et al. 2018, Sci, 361, 482
Maund, J. R., Leloudas, G., Malesani, D. B., et al. 2020, MNRAS, 498, 3730

Maund, J. R., Spyromilio, J., Hoflich, P. A., et al. 2013, MNRAS, 433, L20
Metzger, B. D. 2022, ApJ, 932, 84
Mundell, C. G., Kopač,, D., Arnold, D. M., et al. 2013, Natur, 504, 119
Nakar, E., Piran, T., & Waxman, E. 2003, JCAP, 2003, 005
Pasham, D. R., Cenko, S. B., Levan, A. J., et al. 2015, ApJ, 805, 68
Pasham, D. R., Lucchini, M., Laskar, T., et al. 2023, NatAs, 7, 88
Patat, F. 2017, in Handbook of Supernovae, ed. A. W. Alsabti & P. Murdin (Cham: Springer), 1017
Patat, F., & Romaniello, M. 2006, PASP, 118, 146
Patra, K. C., Lu, W., Brink, T. G., et al. 2022, MNRAS, 515, 138
Perley, D. A., Mazzali, P. A., Yan, L., et al. 2019, MNRAS, 484, 1031
Phinney, E. S. 1989, in IAU Symp. 136, The Center of the Galaxy, ed. M. Morris (Dordrecht: Kluwer Academic), 543
Plaszczynski, S., Montier, L., Levrier, F., & Tristram, M. 2014, MNRAS, 439, 4048
Rees, M. J. 1988, Natur, 333, 523
Rossi, E., Lazzati, D., Salmonson, J. D., & Ghisellini, G. 2004, in ASP Conf. Ser. 312, Gamma-Ray Bursts in the Afterglow Era, ed. M. Feroci et al. (San Francisco, CA: ASP), 460
Roth, N., Rossi, E. M., Krolik, J., et al. 2020, SSRv, 216, 114
Sagiv, A., Waxman, E., & Loeb, A. 2004, ApJ, 615, 366
Sarazin, M., & Roddier, F. 1990, A&A, 227, 294
Saxton, R., Komossa, S., Auchettl, K., & Jonker, P. G. 2020, SSRv, 216, 85
Schlafly, E. F., & Finkbeiner, D. P. 2011, ApJ, 737, 103
Stringer, E., & Lazzati, D. 2020, ApJ, 892, 131
Tadhunter, C., Spence, R., Rose, M., Mullaney, J., & Crowther, P. 2017, NatAs, 1, 0061
Tanvir, N. R., de Ugarte Postigo, A., Izzo, L., et al. 2022, GCN, 31602, 1
Teboul, O., & Shaviv, N. J. 2021, MNRAS, 507, 5340
Toma, K., Ioka, K., & Nakamura, T. 2008, ApJL, 673, L123
van Velzen, S., Holoien, T. W.-S., Onori, F., Hung, T., & Arcavi, I. 2020, SSRv, 216, 124
Wang, L., & Wheeler, J. C. 2008, ARA&A, 46, 433
Wiersema, K., Covino, S., Toma, K., et al. 2014, Natur, 509, 201
Wiersema, K., Higgins, A. B., Levan, A. J., et al. 2020, MNRAS, 491, 1771
Wiersema, K., van der Horst, A. J., Levan, A. J., et al. 2012, MNRAS, 421, 1942
Zabludoff, A., Arcavi, I., La Massa, S., et al. 2021, SSRv, 217, 54
Zauderer, B. A., Berger, E., Soderberg, A. M., et al. 2011, Natur, 476, 425